Magnetic phase transition in V_2O_3 nanocrystals

V. A. Blagojevic,[1] J. P. Carlo,[2,3,*] L. E. Brus,[1] M. L. Steigerwald,[1] Y. J. Uemura,[2] S. J. L. Billinge,[4,5] W. Zhou,[4]
P. W. Stephens,[6] A. A. Aczel,[7] and G. M. Luke[7]

[1]*Department of Chemistry, Columbia University, New York, New York 10027, USA*
[2]*Department of Physics, Columbia University, New York, New York 10027, USA*
[3]*Canadian Neutron Beam Centre, National Research Council, Chalk River, Ontario, Canada K0J 1J0*
[4]*Department of Applied Physics and Applied Mathematics, Columbia University, New York, New York 10027, USA*
[5]*Condensed Matter Physics and Materials Science Department, Brookhaven National Laboratory, Upton, New York 11973, USA*
[6]*Department of Physics, State University of New York at Stony Brook, Stony Brook, New York 11794, USA*
[7]*Department of Physics and Astronomy, McMaster University, Hamilton, Ontario, Canada L8S 4M1*

V_2O_3 nanocrystals can be synthesized through hydrothermal reduction in $VO(OH)_2$ using hydrazine as a reducing agent. Addition of different ligands to the reaction produces nanoparticles, nanorods, and nanoplatelets of different sizes. Small nanoparticles synthesized in this manner show suppression of the magnetic phase transition to lower temperatures. Using muon spin relaxation spectroscopy and synchrotron x-ray diffraction, we have determined that the volume fraction of the high-temperature phase, characterized by a rhombohedral structure and paramagnetism, gradually declines with decreasing temperature, in contrast to the sharp transition observed in bulk V_2O_3.

I. INTRODUCTION

The unique characteristics of the transition-metal oxides make them an extraordinarily diverse class of materials, with properties covering almost all aspects of materials science and solid-state physics. The chemical and physical properties of the group V oxides—vanadium, niobium, and tantalum—show promise for applications in catalysis, electrochemistry, and electrochromical device technology. V_2O_3 has been the subject of many investigations due to a remarkable first-order metal-insulator transition at about 150–160 K,[1,2] from the low-temperature monoclinic[3] into the rhombohedral phase, with an accompanying seven order-of-magnitude increase in conductivity and a shift from antiferromagnetic[4] to paramagnetic[5–8] behavior. The low-temperature phase also exhibits an increase in volume of about 1.6%. The addition of a few percent of Cr,[9] Al,[10] Re,[11] or Mo (Ref. [12]) shifts the conductivity increase to higher temperatures—between 170 and 470 K—depending on doping fraction. These properties make it possible to build temperature sensors and current regulators[13,14] using these materials. Furthermore, V_2O_3 powders have been used in conductive polymer composites[15] and in catalysis.[16] The potential uses of V_2O_3 in the nanocrystalline form will require high chemical and structural purity and well-defined morphology, and careful characterization of the nanoparticle properties.

There have been a few successful syntheses reported of V_2O_3 nanocrystals.[17–21] Zheng *et al.*[18] obtained spherical V_2O_3 nanoparticles through reductive pyrolysis of ammonium oxo-vanadium(IV) carbonate hydroxide, $(NH_4)_2[(VO)_6(CO_3)_4(OH)_9]\cdot 10H_2O$, in a hydrogen flow at 650 °C. Su and Schloegl[19] made V_2O_3 nanoparticles by reducing V_2O_5 crystals in high vacuum (10^{-7} Torr) at 600 °C. Pinna *et al.*[20] discovered a nonaqueous route to V_2O_3 nanocrystals through solvothermal reaction of vanadium(V) triisopropoxide with benzyl alcohol. Benzyl alcohol plays the roles of both reducing agent and surfactant and the reaction is performed at 200 °C under nitrogen. Zhang *et al.*[21] synthesized V_2O_3 nanopowders using thermal decomposition of vanadium(IV) oxalate or mixture of vanadyl hydroxide and ammonium chloride in argon atmosphere at 500 °C. Although there have been no successful syntheses of V_2O_3 nanorods, there have been a few reported syntheses of VO_2 nanorods, which we have used as a starting point.[22]

We report an approach employing hydrothermal reaction in water solution in air to produce V_2O_3 nanorods. We use different ligands to change nanocrystal shape in order to obtain particles, rods, and platelets of V_2O_3. One particular improvement over the previously reported syntheses is that the reaction is not air sensitive. We investigated the magnetic properties of small V_2O_3 nanoparticles and found them to behave differently from the bulk material.

II. SYNTHESIS

The synthesis follows a simple route: the vanadyl hydroxide precursor is heated with hydrazine in an autoclave at 230 °C, in water. The reaction takes 2–14 days, depending on the ionic strength of the solution and the ligand used. We were able to obtain different shapes and sizes of V_2O_3 nanocrystals through change in the ligand as shown in transmission electron microscopy (TEM) images (Fig. 1). Nanorods 40–60 nm in diameter and up to 1 μm in length were produced using succinic acid [Fig. 1(a)]. Electron-diffraction measurements of a single nanorod reveal no variation along the length of the rod. Judging from the TEM images, nanorods account for about 10% of the sample, the rest being nanoparticles. Nanorods produced using ethylene diamine as ligand have diameter of 40–60 nm and length of 300–500 nm [Fig. 1(b)]. Those produced using 2-propanol [Fig. 1(d)] as a ligand were 70–90 nm in diameter and around 700 nm long. These ligands are more selective than succinic acid, with
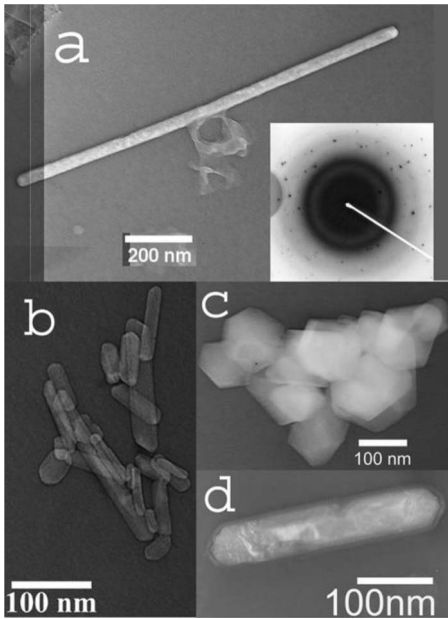
FIG. 1. TEM images of V_2O_3 nanocrystals synthesized using respective ligands: (a) nanorod (succinic acid); (b) nanorods (ethylene diamine); (c) nanoplatelets (ammonium citrate); and (d) nanorod (2-propanol).

nanorods comprising the majority of the sample: the approximate yield of nanorods is around 70% for the reaction using 2-propanol and about 85% for reaction using ethylene diamine as the ligand. Nanoplatelets of 80–200 nm diameter were obtained using ammonium citrate as ligand [Fig. 1(c)]. Finally, nanoparticles (Fig. 2) were produced using 2-propanol as ligand, in a reaction where the precursor is washed to reduce the ionic strength of the solution. The particle size distribution is broad—from less than 10 nm to around 50 nm in diameter.

Thermogravimetric analysis shows a gradual mass loss of about 2% when sample is heated to 860 °C, indicating that the phase is stable and there is no water of crystallization. Elemental analysis of the sample reveals small percentages
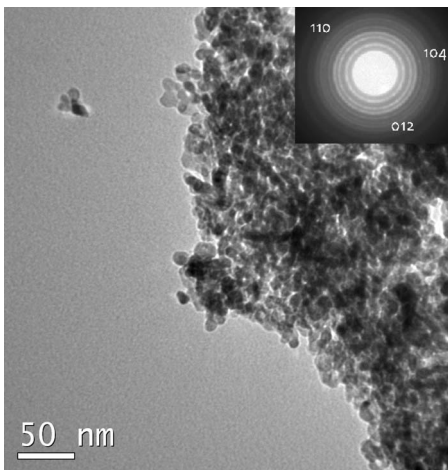

FIG. 2. TEM image of V_2O_3 nanoparticles synthesized using 2-propanol as the ligand.
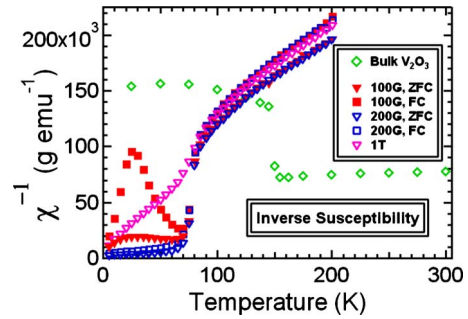

FIG. 3. (Color online) Magnetic susceptibility of V_2O_3 nanoparticles as a function of temperature, in applied fields of 100 G (red solid symbols), 200 G (blue open symbols), and 1 T (violet open symbols), with susceptibility data of McWhan *et al.* (Ref. 2) for the bulk sample (green diamonds) included for reference. Zero-field-cooled and field-cooled measurements are denoted by inverted triangles and squares, respectively.

of carbon and hydrogen and trace amounts of nitrogen and chlorine in the sample. The molar ratios of elements in the sample were consistent with stoichiometric V_2O_3 while the remaining carbon and hydrogen can almost completely be attributed to leftover ligand succinic acid ($C_4H_6O_4$—0.009 molecules per one vanadium), with the remaining hydrogen probably in the form of ammonium. The exact origin of the excess oxygen (0.13 atoms for each vanadium atom) cannot be determined with any degree of certainty.

III. RESULTS

A. Magnetic characterization

The temperature dependence of the magnetic susceptibility of V_2O_3 nanoparticles, measured using a superconducting quantum interference device (SQUID) magnetometer with applied fields of 100 G, 200 G, and 1 T (Fig. 3), shows that there is no large jump in susceptibility near 150 K but a more gradual rise in susceptibility at lower temperatures. This is very different from the behavior of the bulk V_2O_3 crystal, which exhibits a sharp rise in magnetic susceptibility around 150 K as the sample shifts from low-temperature antiferromagnetic ordering to the high-temperature paramagnetic state. In external fields of 100 and 200 G, we see the apparent signature of a sudden change at $T = 80$ K. This, however, can be explained as spin freezing of a small impurity phase or the onset of a slight ferrimagnetic polarization of primarily antiferromagnetic spins, as even the largest values of susceptibility seen at low temperatures correspond to a moment of approximately only 2×10^{-4} μ_B per V site. In addition, while the high-temperature state in bulk V_2O_3 is characterized by a relatively constant Pauli-type susceptibility, the nanopowder sample exhibits distinctly Curie-Weiss-type behavior at high temperatures. In order to further investigate this behavior, we used muon spin relaxation (μSR) spectroscopy.

μSR (Refs. 23 and 24) is an experimental technique based on the implantation of spin-polarized muons in matter and the influence of the atomic, molecular, or crystalline surroundings on the evolution of their spins. It is a pointlike
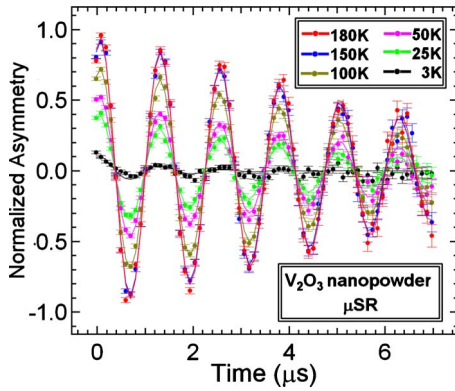
FIG. 4. (Color online) Muon spin relaxation measurements performed in a weak transverse magnetic field of nominally 50 G, as a function of temperature from 3 to 180 K.

magnetic probe in real space, similar to NMR and ESR, and complementary to the frequency space probed by scattering measurements. One key difference between μSR and other related probes such as NMR and ESR is the time window in detecting dynamic phenomena: μSR is sensitive to time scales over the range of 10^{-11}–10^{-5} s. As an added advantage, μSR can be performed in the absence of an external magnetic field.

In a magnetic field, the muon spin precesses at a frequency of about 13.5 kHz G^{-1}; the magnetic moment of the muon is about three times that of the proton, making it a very sensitive magnetic probe. The positive muons used in the measurement, produced by the parity-violating weak decay of pions at rest, exhibit almost 100% initial spin polarization, and decay into a positron and two neutrinos with a mean lifetime of 2.2 μs. The positron is emitted preferentially along the direction of the instantaneous muon spin moment at the time of decay, with a typical overall 20–30 % asymmetry between the directions parallel and antiparallel to the muon spin at time of decay. The time-dependent asymmetry of detected decay positrons correlates directly to the time evolution of the spins of the implanted muons, and thus to the internal local-field distribution in the sample.

Temperature-dependent μSR measurements[25,26] were performed at the M15 beamline at TRIUMF in a transverse field of 50 G in the temperature range of 3–180 K (Fig. 4) using the HiTime spectrometer. The long-lived oscillating component represents muons in paramagnetic environments, while precessing muon spins in the antiferromagnetic environment quickly dephase due to local fields, resulting in rapid relaxation of the initial muon spin asymmetry. The data indicate that the onset of magnetic ordering occurs at different temperatures in different parts of the sample (presumably corresponding to different particle sizes). This is in stark comparison to the rapid and hysteretic transition previously observed in μSR measurements of bulk V$_2$O$_3$.[27]

B. Structural characterization

Bulk V$_2$O$_3$ exhibits concurrent magnetic, structural, and metal-insulator phase transitions. To attempt to correlate the observed magnetic properties of V$_2$O$_3$ nanopowder with any structural changes, we performed synchrotron x-ray diffraction (XRD) measurements on our sample, as well as on commercially prepared bulk powder. These measurements were conducted at beamline X16C at the National Synchrotron Light Source (NSLS) at Brookhaven National Laboratory (BNL), with the samples packed in quartz capillaries and measured using x rays of wavelength 0.698955 Å. Complete data sets from 10° to 40° were collected for the bulk sample as a function of temperature, and complete data sets at 20 and 300 K, as well as shorter scans at intermediate temperatures, were taken for the nanopowder sample.

The bulk data were analyzed using the FULLPROF Rietveld refinement program,[28] and the data were fit to a rhombohedral high-temperature phase and a monoclinic low-temperature phase consistent with earlier published results. We confirm that, as in earlier published results,[1,2] the transition occurs quite rapidly, and is associated with coexistence of the high- and low-temperature phases over a narrow range of temperatures, with the transition temperature exhibiting significant hysteresis, as expected for a strongly first-order phase transition.

In the nanopowder sample, broadening of Bragg peaks and a high background made Rietveld refinement impossible and necessitated much longer integration times for data collection. Measurements of the empty quartz capillary showed that this large background phase is in fact intrinsic to the sample, although it is temperature independent, and its origin remains unknown.

As a result of these limitations, we chose to focus on the region around 24° corresponding to the bulk [116] peak. In the bulk sample, this peak exhibits a threefold splitting as the sample transitions from the rhombohedral to the monoclinic phase. Although the [116] peak in the nanopowder sample overlaps with a broad background peak, this background is temperature independent and may be subtracted from the data after being fitted to a temperature-independent Gaussian. The sample signal was fit to a sum of a single Gaussian representing the high-temperature phase, and a sum of three Gaussians representing the low-temperature phase. Our results are shown in Fig. 5, revealing the gradual dropoff of the high-temperature peak intensity with decreasing temperature, and a corresponding rise in the more diffuse scattering representing the low-temperature phase. While limitations of the data do not allow us to quantitatively analyze the structure of the low-temperature phase, we can determine that coexistence of the high- and low-temperature phases does occur over a wide temperature range similar to that where the high- and low-temperature magnetic phases were seen to coexist in the μSR measurements.

This motivated us to compare the relative phase fractions of high- and low-temperature phases obtained by the two techniques. In Fig. 6 we show with red filled squares the temperature dependence of the oscillating asymmetry component of muon spin relaxation, giving a relative measure of volume fraction of the paramagnetic region, and with blue open squares the temperature dependence of the integrated intensity coming from the high-temperature structural phase observed by x-ray diffraction. For comparison, the high-temperature rhombohedral phase fraction observed by x-ray diffraction in the bulk material is shown for both warming
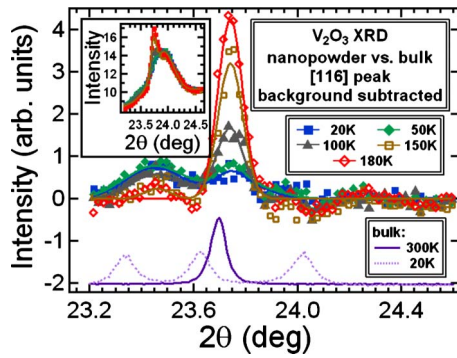
FIG. 5. (Color online) XRD Data around the [116] peak. The nanopowder data are shown with a temperature-independent background (seen as the broad peak in the inset) subtracted. Comparison data for the bulk material is shown at the bottom (arbitrary intensity offset). The high-temperature phase is represented by the single peak near 23.75°, whereas the low-temperature phase is seen in several broad peaks, most noticeably near 23.4°. A gradual crossover is seen between the two phases as a function of temperature.

and cooling cycles. Both methods reveal that the volume fraction of the rhombohedral/paramagnetic phase increases gradually with increasing temperature and levels off after $T \sim 150$ K, suggesting that these signals come from the same regions of the material.

IV. DISCUSSION

A. Synthesis

The vanadyl hydroxide precursor obtained through different processes yields different results. When it is obtained by reducing V_2O_5 with hydrazine, the reaction yields V_2O_3. When the precursor is prepared by precipitation from $VOSO_4$ solution without a reducing agent, the reduction to vanadium(III) does not occur. However, when the same reaction is performed with the addition of hydrazine to the precursor before placing it in the autoclave, the result is V_2O_3. This suggests that excess hydrazine is acting as a reducing agent in the final step of the reaction, reducing vana-

dium(IV) to vanadium(III). In fact, there is evidence in the literature[19] suggesting that if the molar ratio of hydrazine to vanadium is 1:1, allowing only for reduction from vanadium(V) to vanadium(IV), that the product of hydrothermal reaction is $VO_2 \cdot xH2O$. Reactions performed at temperatures below 200 °C failed to produce V_2O_3, suggesting that there is a minimum temperature required for vanadium reduction under hydrothermal conditions. 2-propanol accelerates the reaction as compared to equivalent ligand-free reaction: the reaction with 2-propanol as a ligand takes 1 day to produce V_2O_3 at 230 °C while a ligand-free reaction under the same conditions takes 3 days. There are two possible explanations, which are not mutually exclusive: 2-propanol might be acting as a weak reducing agent, thus accelerating vanadium reduction, or the acceleration might simply come from the fact that the 2-propanol reaction produces much smaller particles than any other we have performed. Small particles might be reduced more quickly simply because they would expose a larger surface area to hydrazine in the solution. It is also interesting to note that the ionic strength of the solution appears to have an effect on both the reaction time and the morphology of the product. We can look at two reactions using 2-propanol as a ligand and differ only in the fact that, in the second one, the precursor was washed with water to reduce ionic strength. The first reaction takes eight times longer to complete and produces a mix of nanorods and nanoparticles (70–90 nm in diameter). The second reaction produces only small nanoparticles (7–50 nm in diameter). We also observed that using ethylene diamine as a ligand requires significantly longer reaction time (14 days) than other reactions at the same conditions (7 days). This suggests that ethylene diamine slows down the reaction, possibly by stabilizing vanadium(IV).

B. Characterization

Magnetic measurements on V_2O_3 nanoparticles synthesized using 2-propanol as ligand show that the magnetic transition (from antiferromagnetic to paramagnetic) appears to be occurring gradually as the temperature increases, rather than abruptly as it does in the bulk crystals. SQUID measurements (Fig. 3) show a gradual inflection in susceptibility below 150 K, and no bulklike sharp transition at 150–160 K. Analysis of the muon spin relaxation and x-ray diffraction measurements (Fig. 6) show that the volume of the paramagnetic/rhombohedral region increases steadily with increasing temperature, suggesting a particle size dependence on transition temperature. By the time the temperature reaches 150 K the curve of the asymmetry amplitude dependence is almost leveled off. The asymmetry value at 180 K is about 0.16, indicating that all of the nanoparticles are in the paramagnetic state. The x-ray diffraction results largely follow this trend, indicating a gradual decrease in the high-temperature phase fraction with decreasing temperature. Characterization of the crystalline phases is impossible, however, due to the limitations of the data, primarily from a large but temperature-independent signal arising from the sample itself. We are thus limited to a semiquantitative estimate of the phase fractions, which display the same trend as the magnetic data.
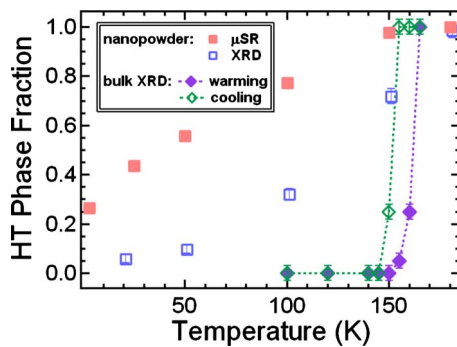

FIG. 6. (Color online) Comparison of high-temperature phase fractions determined by μSR (red solid squares) and XRD (blue open squares). Corresponding phase fractions determined by XRD on bulk V_2O_3 on warming (violet filled diamonds) and cooling (green open diamonds) are shown for reference.

Magnetic ordering of the monoclinic phase of bulk V_2O_3 has been revealed by polarized neutron-scattering experiments to be ferromagnetic in planes perpendicular to the [010] direction while adjacent planes are antiferromagnetically coupled.[29,30] This results in zero overall magnetic moment, event though individual layers have a relatively high moment of 1.2 μ_B per vanadium atom. Experiments[31] have shown that the magnetic transition can be shifted to a temperature below 150 K by application of pressure. At a pressure of about 15 kbar the magnetic transition decouples from the metal-insulator transition, and by about 26 kbar, both phase transitions are completely suppressed.

C. Possible size dependence of transition temperature

It is apparent from the XRD data that the high-temperature [116] peak in the nanopowder sample is shifted to an angle about 0.2% larger than is seen in the bulk material, indicating that the lattice parameters in the nanopowder sample are correspondingly smaller than in the bulk. Furthermore, the [116] peak in the bulk material exhibits significant broadening relative to its counterpart in the bulk. Bragg peak widths can be ascribed to several causes, including instrumental resolution, finite particle size, variation in lattice parameters throughout different parts of the specimen, and microstrain effects. The width of the broadened nanopowder peak, well approximated by a Gaussian, may be parametrized as $\sigma_{NP}^2 = \sigma_{int}^2 + \sigma_{exc}^2$, where σ_{int} is the intrinsic width approximated by the width of the peak in the bulk material, and σ_{exc} defined as the "excess width" due to the remaining factors.

In our current data set, the full width at half maximum (FWHM) in 2Θ of the bulk peak is 0.152° while that of the nanopowder sample is 0.222°; this leaves an excess FWHM due to broadening of 0.162°. If we ascribe the entirety of this broadening to the finite size of the nanoparticles, we find by application of the Debye-Scherrer formula[32] $L = K\lambda/\beta \cos\Theta$ (where L represents the particle size, λ the wavelength, Θ the Bragg angle, and β the peak FWHM in radians) that the observed width corresponds to an average particle size of 23 nm, in the lower midrange of the 10–50 nm (based on TEM images) particle size distribution, assuming a typical Debye-Scherrer constant value $K=0.9$. Unfortunately, it is impossible to distinguish between the varying sources of broadening in the current data set, nor is it possible to determine whether finite size effects alone are sufficient to explain the observed broadening.

One intriguing interpretation of the range of transition temperatures observed is that it arises from the relatively wide particle size distribution in the sample. In particular, since progressively smaller nanoparticles have an increasingly large ratio of surface area to volume, it is expected that surface tension would hold smaller particles in greater compression, resulting in smaller lattice parameters. If the lattice parameters are a critical determinant of the transition temperature, the transition temperature and its range over the sample may be determined from measurement of the lattice parameters.

Finger and Hazen[33] have determined the variation in lattice parameters of bulk V_2O_3 under applied pressure up to 50 kbar, from which we may compute the [116] peak d spacing as a function of pressure. McWhan *et al.*[2] have characterized the depression of the transition temperature as a function of applied pressure, finding that the transition temperature drops linearly at a rate of approximately −5 K/kbar up to about 16 kbar, then more rapidly decreases toward zero at a sample-dependent critical pressure of 20–26 kbar. Combining these results, one may estimate approximately the transition temperature as a function of [116] d spacing. Using this relation, we find that the centroid of the nanopowder [116] peak corresponds to an effective pressure of 14 kbar and an estimated transition temperature of 85 K. If there is a spread of lattice parameter values throughout the sample, it would also follow that this transition should be smeared out, with portions of the sample exhibiting smaller lattice parameters (corresponding to a higher effective pressure) undergoing the transition at lower temperatures, and portions of the sample exhibiting larger lattice parameters (corresponding to effective pressures closer to zero) undergoing the transition at higher temperatures. This is roughly consistent with our μSR and XRD observations indicating coexistence of the high- and low-temperature phases from base temperature up to over 150 K, although uncertainties about the precise distribution of particle shapes and sizes and unknown strain effects prevent a more quantitative comparison.

Finally, since magnetic ordering in the low-temperature phase is long range, and because of the dimensions of the nanoparticles, the magnetic transition caused by the antiparallel alignment of magnetic moments in adjacent planes might not necessarily occur concurrently with the structural transition. Further investigation is required to confirm these findings.

V. CONCLUSIONS

We present an approach for synthesis of V_2O_3 nanocrystals via hydrothermal reduction. Unlike any other reported syntheses, this reaction is done in water and under ambient atmosphere. We have obtained nanocrystals of varied shapes and sizes through choice of ligand.

The magnetic properties of V_2O_3 nanoparticles have been measured with respect to temperature using susceptibility and muon spin relaxation, and it is found that unlike the behavior in the bulk material, there is a gradual onset of magnetic order with decreasing temperature.

Additionally, the structural properties of V_2O_3 nanoparticles have been studied using synchrotron x-ray diffraction. While a full structural refinement of the data was impossible due to the large background signal, clearly a high-temperature phase and a low-temperature phase trade off with one another as a function of temperature. Both the magnetic and the structural results indicate coexistence of high- and low-temperature phases over a broad temperature range, with qualitative agreement between the phase fractions determined by magnetic and by structural measurements. The high-temperature phase is consistent with the observed bulk rhombohedral phase, although the low-temperature phase structure cannot be deduced with the available data.

These results suggest a correspondence between lattice parameters and transition temperature, with an intriguing explanation being that a particle size dependence to the transition temperature exists due to compression by surface tension. However, the relatively wide size distribution of the nanoparticle sample precludes any definitive conclusions, which await further investigation.

*Author to whom correspondence should be addressed; jeremy.carlo@nrc-cnrc.gc.ca

[1] A. I. Frenkel, E. A. Stern, and F. A. Chudnovsky, Solid State Commun. **102**, 637 (1997).

[2] D. B. McWhan, A. Menth, J. P. Remeika, W. F. Brinkman, and T. M. Rice, Phys. Rev. B **7**, 1920 (1973).

[3] P. D. Dernier and M. Marezio, Phys. Rev. B **2**, 3771 (1970).

[4] J. B. Goodenough, J. Appl. Phys. **39**, 403 (1968).

[5] P. H. Carr and S. Foner, J. Appl. Phys. **31**, S344 (1960).

[6] D. J. Arnold and R. W. Mires, J. Chem. Phys. **48**, 2231 (1968).

[7] S. A. Carter, T. F. Rosenbaum, J. M. Honig, and J. Spalek, Phys. Rev. Lett. **67**, 3440 (1991).

[8] M. Greenwood, R. W. Mires, and A. R. Smith, J. Chem. Phys. **54**, 1417 (1971).

[9] C. Smerdou, I. M. Anton, J. Plana, R. Curtis, L. Enjuanes, H. R. Kokabi, F. Studer, and M. Toulemonde, Nucl. Instrum. Methods Phys. Res. B **111**, 75 (1996).

[10] M. G. Joshi and M. J. Honig, Rev. Chim. Miner. **19**, 251 (1982).

[11] T. Suzuki, M. Ogino, T. Yoshizuka, K. Kunihara, and K. Tsuda, Adv. Sci. Technol. (Faenza, Italy) **17**, 135 (1999).

[12] C. Tenailleau, E. Suard, J. Rodriguez-Carvajal, M. P. Crosnier-Lopez, and P. Lacorre, Chem. Mater. **14**, 3569 (2002).

[13] E. Andrich, Electron. Appl. **26**, 123 (1996).

[14] S. R. Perkins, A. Ruegg, and M. Fischer, Adv. Ceram. **7**, 166 (1983).

[15] Y. Pan, G. Wu, and X. Yi, J. Mater. Sci. **29**, 5757 (1994).

[16] G. van der Lee, B. Schuller, H. Post, T. L. F. Favre, and V. Ponec, J. Catal. **98**, 522 (1986).

[17] O. Toshiyuki, I. Yasuhiro, and R. K. Kenkyu, J. Photopolym. Sci. Technol. **10**, 211 (1997).

[18] C. Zheng, X. Zhang, S. He, Q. Fu, and D. Lei, J. Solid State Chem. **170**, 221 (2003).

[19] D. S. Su and R. Schloegl, Catal. Lett. **83**, 115 (2002).

[20] N. Pinna, M. Antonietti, and M. Niederberger, Colloids Surf., A **250**, 211 (2004).

[21] K. Zhang, X. Sun, G. Lou, X. Liu, H. Li, and Z. Su, Mater. Lett. **59**, 2729 (2005).

[22] Z. Gui, R. Fan, W. Mo, X. Chen, L. Yang, S. Zhang, Y. Hu, Z. Wang, and W. Fan, Chem. Mater. **14**, 5053 (2002).

[23] A. Schenck, *Muon Spin Rotation Spectroscopy* (Adam Hilger, Bristol, 1985).

[24] *Muon Science: Proceedings of the Fifty First Scottish Universities Summer School in Physics*, edited by S. L. Lee, S. H. Kilcoyne, and R. Cywinski (Institute of Physics, Bristol, 1998).

[25] Y. J. Uemura *et al.*, Nat. Phys. **3**, 29 (2007).

[26] A. T. Savici *et al.*, Phys. Rev. B **66**, 014524 (2002).

[27] Y. J. Uemura, T. Yamazaki, Y. Kitaoka, M. Takigawa, and H. Yasuoka, Hyperfine Interact. **17**, 339 (1984).

[28] J. Rodríguez-Carvajal, Physica B **192**, 55 (1993).

[29] R. M. Moon, Phys. Rev. Lett. **25**, 527 (1970).

[30] A. Heidemann, Z. Phys. **238**, 208 (1970).

[31] S. A. Carter, T. F. Rosenbaum, M. Lu, H. M. Jaeger, P. Metcalf, J. M. Honig, and J. Spalek, Phys. Rev. B **49**, 7898 (1994).

[32] A. L. Patterson, Phys. Rev. **56**, 978 (1939).

[33] L. W. Finger and R. M. Hazen, J. Appl. Phys. **51**, 5362 (1980).